

Strong cosmological constraints on the neutrino magnetic moment

Pierluca Carenza^{1,*}, Giuseppe Lucente^{2,3,4,5,†}, Martina Gerbino^{6,‡},
Maurizio Giannotti^{7,8,§} and Massimiliano Lattanzi^{6,||}

¹*The Oskar Klein Centre, Department of Physics, Stockholm University, Stockholm 106 91, Sweden*

²*Dipartimento Interateneo di Fisica “Michelangelo Merlin”, Via Amendola 173, 70126 Bari, Italy*

³*Istituto Nazionale di Fisica Nucleare—Sezione di Bari, Via Orabona 4, 70126 Bari, Italy*

⁴*Kirchhoff-Institut für Physik, Universität Heidelberg, Im Neuenheimer Feld 227,
69120 Heidelberg, Germany*

⁵*Institut für Theoretische Physik, Universität Heidelberg, Philosophenweg 16,
69120 Heidelberg, Germany*

⁶*Istituto Nazionale di Fisica Nucleare, Sezione di Ferrara, via Giuseppe Saragat 1, I-44122 Ferrara, Italy*

⁷*Centro de Astropartículas y Física de Altas Energías (CAPA), Universidad de Zaragoza,
Zaragoza 50009, Spain*

⁸*Department of Chemistry and Physics, Barry University, 11300 NE 2nd Avenue,
Miami Shores, Florida 33161, USA*

 (Received 17 January 2023; revised 8 January 2024; accepted 7 June 2024; published 8 July 2024)

A sizable magnetic moment for neutrinos would be evidence of exotic physics. In the early Universe, left-handed neutrinos with a magnetic moment would interact with electromagnetic fields in the primordial plasma, flipping their helicity and producing a population of right-handed (RH) neutrinos. In this work, we present a new calculation of the production rate of RH neutrinos in a multicomponent primordial plasma and quantify their contribution to the total energy density of relativistic species at early times, stressing the implications of the dependence on the initial time for production. We find that current cosmological data exclude values of the magnetic moment $\mu \gtrsim 1.6 \times 10^{-11} \mu_B$, while future cosmological experiments will be able to probe nonthermal production of RH neutrinos, becoming competitive with stellar limits.

DOI: 10.1103/PhysRevD.110.023510

I. INTRODUCTION

The existence of a sizable neutrino magnetic moment (NMM) μ is a fascinating possibility, which has generated a vivid interest in experimental and phenomenological communities in the recent years. If equipped with (transition) magnetic moments, then neutrinos would couple to photons through the effective Lagrangian terms,

$$L = -\frac{1}{2} \mu^{ij} \bar{\psi}_i \sigma_{\alpha\beta} \psi_j F^{\alpha\beta}, \quad (1)$$

where ψ is the neutrino field, F the electromagnetic field tensor, α, β are Lorentz indices, and i, j are the flavor indices. The first experimental constraint goes back to the very neutrino discovery experiment by Cowan and Reines [1]. Analyzing electron recoil spectra in (anti-) neutrino electron scattering, the authors derived the bound $\mu \lesssim 10^{-9} \mu_B$, where $\mu_B = e/2m_e$ denotes the Bohr magneton. Later searches gave considerably stronger constraints [2–9]. The current experimental sensitivity is slightly below $10^{-11} \mu_B$. Although neutrinos with a Dirac mass are expected to have a magnetic moment [10], this is predicted to be quite small, $\mu \approx 3 \times 10^{-19} \times (m_\nu/1 \text{ eV}) \mu_B$. Thus, a sizable magnetic moment would be evidence of exotic physics. Furthermore, even though several extensions of the standard model predict a larger neutrino magnetic moment, the predictions change substantially for Dirac and Majorana neutrinos, with the latter allowed more naturally to have a large μ [11–14]. Hence, a discovery of a sufficiently large magnetic moment would also shed light on the nature of the neutrino field.

A nonvanishing neutrino magnetic moment would have profound astrophysical and cosmological consequences.

*Contact author: pierluca.carenza@fysik.su.se

†Contact author: giuseppe.lucente@ba.infn.it

‡Contact author: gerbinom@fe.infn.it

§Contact author: mgiannotti@unizar.es

||Contact author: lattanzi@fe.infn.it

Published by the American Physical Society under the terms of the Creative Commons Attribution 4.0 International license. Further distribution of this work must maintain attribution to the author(s) and the published article's title, journal citation, and DOI. Funded by SCOAP³.

Stellar evolution provides some of the strongest bounds on μ . The resulting tree-level neutrino-photon interaction contributes substantially to several cooling mechanisms in stars (see, e.g., Ref. [15] for a comprehensive discussion), most notably to the plasmon decay $\gamma \rightarrow \bar{\nu}\nu$. A recent analysis of the cooling of red giant stars [16] provided the constraint $\mu \lesssim 1.2 \times 10^{-12} \mu_B$, about a factor of 5 below the current experimental sensitivity.¹

Furthermore, for Dirac neutrinos, a nonvanishing magnetic moment would induce the production of right-handed (RH) neutrinos via spin-flip of left-handed (LH) neutrinos in an external electromagnetic field. For a supernova, where LH neutrinos are trapped and RH neutrinos are not, this would imply a very efficient energy loss mechanism [17–19]. Spin-flip processes may also play a significant role in the early Universe, given the large number of charged particles generating electromagnetic fields required for this process to take place. The production of RH neutrinos in this case would affect the predictions of the light-elements' abundances because of the increased number of relativistic degrees of freedom N_{eff} [20–23]. In the past, the above observables were used to derive the constraint $\mu \lesssim 6.2 \times 10^{-11} \mu_B$ [24], a result considerably less stringent than the current astrophysical limits. The analysis of Ref. [24], however, did not account for spin-flip processes in the electromagnetic field generated by charged particles other than electrons and positrons. In the early Universe, especially above the phase transition of the quantum chromodynamics (QCD), we expect a large number of charged particles and thus more efficient spin-flip processes. Current and upcoming cosmological surveys severely constrain N_{eff} , leading to tighter bounds on μ . A recent analysis in this direction was performed in Ref. [25]. The study presented a detailed calculation of the neutrino chirality flipping rate in a thermal plasma, including a careful and consistent consideration of soft scattering and the plasmon effect in finite temperature field theories. This analysis found that a NMM above $2.7 \times 10^{-12} \mu_B$ is excluded by current cosmic microwave background (CMB) and big bang nucleosynthesis (BBN) measurements of ΔN_{eff} . Here, we revisit and improve on this calculation of RH neutrino production in the early Universe, extensively discussing the cosmological implications.

In Sec. II, we discuss the thermal field theory methods employed in the calculation of the rate. In Sec. III, we discuss the cosmological implications of a sizable NMM. Moreover, we show that the requirement of not exceeding

¹Different observables could be sensitive to different combinations of the elements of the magnetic moment matrix μ^{ij} . For example, terrestrial experiments using reactor sources (electron antineutrinos) are sensitive to the μ^{ei} components. On the other hand, bounds based on energy loss in stars, such as the one in Ref. [16], are sensitive to all of the combinations of μ^{ij} .

the number of effective relativistic species allowed by cosmological observations results in a strong constraint on μ . Finally, in Sec. V, we conclude by discussing incoming cosmological experiments able to probe the freeze-in regime of RH neutrino production. Two appendices follow.

II. RH NEUTRINO PRODUCTION RATE

Neutrinos with a magnetic moment interact with the surrounding plasma through current-current interactions with the electromagnetic fields generated by charged particles. Information about the medium and its electromagnetic fluctuations is encoded in the imaginary part of the photon polarization tensor $\Pi_{\mu\nu}$, obtained at one loop by summing over loops with all the charged particles in a plasma. Reference [24] calculated the net RH neutrinos production rate Γ in a hot plasma using the thermal field theory approach,

$$\begin{aligned} \Gamma &= \frac{\mu^2}{2\pi} \int_0^\infty dk k \int_{-\infty}^\infty dk_0 \theta(-K^2(K^2 + 4pk_0 + 4p^2)) \\ &\epsilon(k_0) \frac{K^4}{k^2} \left[\frac{\epsilon(k_0)}{e^{\frac{|p_0+k_0|}{T}} + 1} + \frac{\epsilon(p_0+k_0)}{e^{\frac{|k_0|}{T}} - 1} \right. \\ &\quad \left. + \epsilon(p_0+k_0)\theta(-k_0) - \epsilon(k_0)\theta(-k_0-p_0) \right] \\ &\times \left[\left(1 + \frac{k_0}{p} + \frac{K^2}{4p^2}\right) \mathcal{A}_T(K) - \left(1 + \frac{k_0}{2p}\right)^2 \mathcal{A}_L(K) \right], \end{aligned} \quad (2)$$

where (p_0, p) is the neutrino four-momentum, $K = (k_0, k)$ the photon four-momentum, T the temperature of the thermal bath, θ the Heaviside theta function, ϵ the sign function, and the sources of electromagnetic fields are encoded in the photon spectral functions $\mathcal{A}_{T,L}$, defined as

$$\mathcal{A}_{T,L}(K) = -\frac{1}{\pi} \frac{\text{Im}\Pi_{T,L}}{|K^2 - \text{Re}\Pi_{T,L}|^2 + |\text{Im}\Pi_{T,L}|^2}, \quad (3)$$

in terms of the transverse Π_T and longitudinal Π_L components of the photon polarization tensor. In a single component plasma with a fermion of mass m_f and charge e_f the photon polarization tensor is given by [26]

$$\begin{aligned} \Pi_L(m_f, e_f) &= -\frac{K^2}{k^2} u^\mu u^\nu \Pi_{\mu\nu}, \\ \Pi_T(m_f, e_f) &= -\frac{1}{2} \Pi_L + \frac{1}{2} g^{\mu\nu} \Pi_{\mu\nu}, \end{aligned} \quad (4)$$

where $g^{\mu\nu}$ is the metric tensor, u^μ the plasma four-velocity, which in the rest frame reduces to $u^\mu = (1, 0, 0, 0)$, while

$$\begin{aligned}
 u^\mu u^\nu \Pi_{\mu\nu} = e_f^2 \int \frac{dq q^2}{2E_q \pi^2} \frac{1}{e^{E_q/T} + 1} & \left[2 - \frac{(2E_q + k_0)^2 - k^2}{4qk} \ln \left(\frac{k_0^2 - k^2 + 2(E_q k_0 + qk)}{k_0^2 - k^2 + 2(E_q k_0 - qk)} \right) \right. \\
 & \left. + \frac{(2E_q - k_0)^2 - k^2}{4qk} \ln \left(\frac{k_0^2 - k^2 - 2(E_q k_0 + qk)}{k_0^2 - k^2 - 2(E_q k_0 - qk)} \right) \right], \quad (5)
 \end{aligned}$$

and

$$\begin{aligned}
 g^{\mu\nu} \Pi_{\mu\nu} = 2e_f^2 \int \frac{dq q^2}{2E_q \pi^2} \frac{1}{e^{E_q/T} + 1} & \left[2 + \frac{k_0^2 - k^2 + 2m_f^2}{4qk} \ln \left(\frac{k_0^2 - k^2 + 2(E_q k_0 - qk)}{k_0^2 - k^2 + 2(E_q k_0 + qk)} \right) \right. \\
 & \left. - \frac{k_0^2 - k^2 + 2m_f^2}{4qk} \ln \left(\frac{k_0^2 - k^2 - 2(E_q k_0 - qk)}{k_0^2 - k^2 - 2(E_q k_0 + qk)} \right) \right], \quad (6)
 \end{aligned}$$

with $E_q = \sqrt{q^2 + m_f^2}$ the energy of the fermion in the loop. Note that this formalism includes all the effects proportional to μ^2 , as plasmon decay and electron-positron annihilation in neutrino-antineutrino pairs, spin-flip transitions, and Cherenkov processes [24]. Among these, plasmon decay is negligible in the early Universe [25]. In a multicomponent plasma, the full polarization tensor is obtained by summing Eqs. (5) and (6) over all the species f :

$$\Pi_{T,L} = \sum_f \Pi_{T,L}(m_f, e_f). \quad (7)$$

Our study extends the previous results [24], valid for a monocomponent plasma of massless electrons, to the more realistic case of a multicomponent primeval plasma, including finite mass effects. We underline that the numerical integration of the production rate in Eq. (2) is stiff when the photon approaches the on-shell condition. In this limit, the imaginary part of the polarization tensor vanishes, $\text{Im}\Pi_{T,L} \rightarrow 0$, and Eq. (3) reduces to a Dirac delta function $\delta(K^2 - \text{Re}\Pi_{T,L})$. Therefore, we can replace the integration over the photon energy with just the contribution coming from the on-shell photon. This is at the origin of the peak in the production rate Γ at low values of the neutrino momentum ($p/T \ll 1$) shown in the upper panel of Fig. 1. However, this affects only slightly our results, which depend mostly on large momenta. As expected, the rate increases with the number of charged species in the plasma, as encoded by the effective number of entropy degrees of freedom $g_{*,s}(T)$. We find that $\alpha^{-1} \mu^{-2} T^{-3} \Gamma(p/T) / \sqrt{g_{*,s}(T)}$ is approximately constant for $T \gtrsim 10$ MeV.

In the lower panel of Fig. 1 we show the full shape of $\langle \Gamma \rangle / (\alpha \mu^2 T^3)$, obtained by averaging over a thermal neutrino distribution. The series of drops below $T \approx 100$ GeV are due to changes in $g_{*,s}(T)$. Our calculation smoothly interpolates between different temperatures, leading to $\langle \Gamma \rangle = 1.91 \alpha \mu^2 T^3$, where the brackets denote a thermal average over a plasma containing only electrons at $T = 10$ MeV, and $\langle \Gamma \rangle = 6.04 \alpha \mu^2 T^3$ at $T = 100$ GeV. This result can be compared to [25], which evaluated the

RH neutrino production rate using a different approach, obtaining $\langle \Gamma \rangle = 6.47 \alpha \mu^2 T^3$.

III. COSMOLOGICAL IMPLICATIONS

The phase-space distribution function for RH neutrinos $f^R(t, q)$ of comoving momentum $q = ap$, with a the

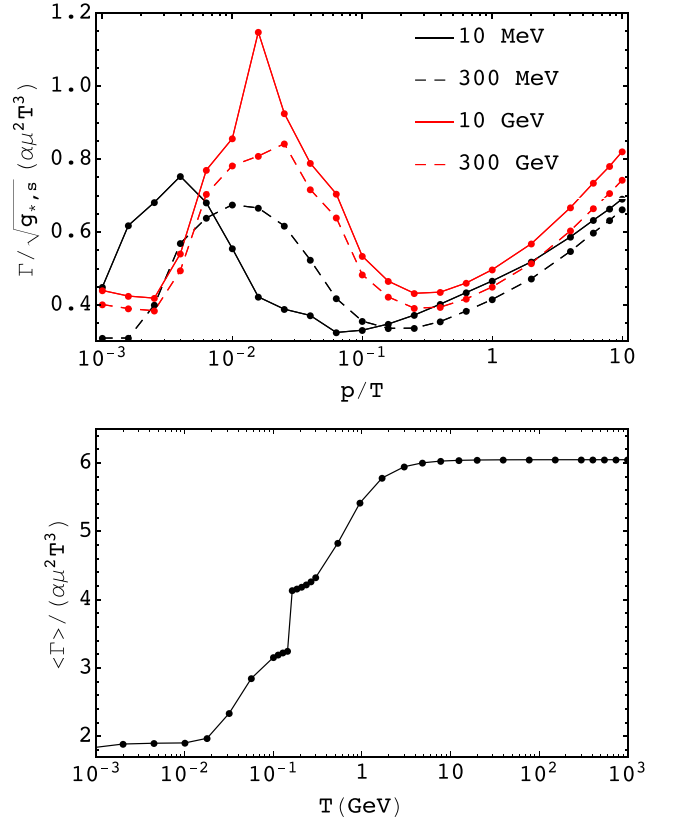


FIG. 1. Upper panel: production rate Γ for RH neutrinos as a function of the neutrino momentum in terms of p/T , for different values of temperature. The lines are a linear interpolation between the values of p/T at which the rate is computed, marked by circles. Lower panel: thermally-averaged production rate $\langle \Gamma \rangle$ as a function of temperature. The solid curve shows a linear interpolation between the values of T at which the rate is computed, marked by circles.

cosmological scale factor, evolves according to the Boltzmann equation [24]:

$$\partial_t f^R = -\Gamma(f^R - f^{\text{eq}}), \quad (8)$$

where $f^{\text{eq}}(t, q)$ is the (local) equilibrium distribution function. We take f^{eq} to be the distribution function of the left-handed neutrinos f_ν , which are kept in thermal equilibrium with the primordial plasma at temperature T by the weak interactions

$$f^{\text{eq}} \simeq f_\nu = \frac{1}{\exp\left(\frac{q}{dT}\right) + 1}. \quad (9)$$

The evolution equation is solved for f^R over a grid of values of the comoving momentum, together with the initial condition $f_{\text{in}}^R = 0$, i.e., no initial population of RH neutrinos.

The initial integration time, corresponding to a temperature T_{in} , can be chosen freely and may affect the outcome. The integration always ends at $T_{\text{fin}} = 10$ MeV as, at lower temperatures, the spin-flip rate becomes rapidly negligible, and no more RH neutrinos are produced.

The ratio $\langle\Gamma\rangle/H$, H being the Hubble parameter, scales as $\mu^2 T$ in the radiation-dominated era, for constant effective number of entropy degrees of freedom g_{*s} . Thus, the production of RH neutrinos is dominated by the high-temperature regime, and our results might depend on the initial time chosen for the integration. Defining the decoupling temperature T_d through $\langle\Gamma\rangle/H|_{T_d} = 1$, RH neutrinos quickly thermalize roughly at the initial time, if $T_{\text{in}} \gg T_d$, and their final abundance will be independent of T_{in} . In this case, the abundance relative to active neutrinos depends only on entropy injections in the plasma happening at $T \lesssim T_d$. Note that since $\langle\Gamma\rangle/H \propto T$, it takes some time for decoupling to complete, and significant entropy injection to the RH component can take place even at $T < T_d$. On the other hand, if $T_{\text{in}} \lesssim T_d$, then the abundance of RH neutrinos depends on T_{in} , since their production happens out-of-equilibrium, in a “freeze-in” kind of process, with T_{in} setting the time interval during which RH neutrinos can be efficiently produced. Both regimes are correctly captured by solving the Boltzmann equation, as discussed in Appendix A. The extra contribution² ΔN_{eff} to N_{eff} due to the population of a single species of RH neutrinos at a given time is obtained as

$$\Delta N_{\text{eff}}(T) = \frac{\int dp p^3 f^R(p, T)}{\int dp p^3 f_\nu(p, T)}. \quad (10)$$

²In the standard cosmological model, the number of relativistic degrees of freedom beyond photons is given by active neutrinos only. The predicted value is $N_{\text{eff}} = 3.044$ [27–31], and we define $\Delta N_{\text{eff}} \equiv N_{\text{eff}} - 3.044$.

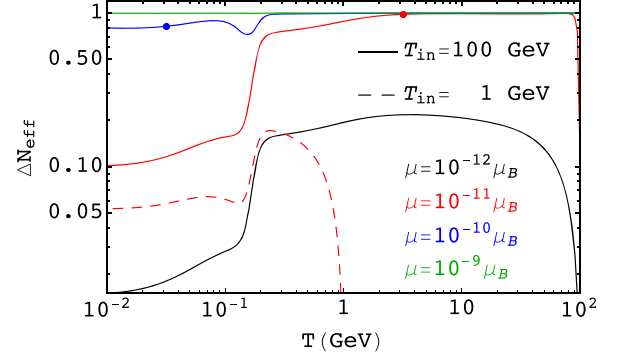


FIG. 2. Evolution of ΔN_{eff} due to the population of a single species of RH neutrinos, as per Eq. (10). The solid lines are obtained for $T_{\text{in}} = 100$ GeV and different values of μ , while the dashed line for $\mu = 10^{-11} \mu_B$ and $T_{\text{in}} = 1$ GeV. The dots mark the values of the decoupling temperature T_d .

In Fig. 2, we show the evolution of $\Delta N_{\text{eff}}(T)$ for different values of μ setting the initial temperature to $T_{\text{in}} = 100$ GeV. On each curve, we mark with a small circle the corresponding decoupling temperature. There are no circles on the curves for $\mu = 10^{-12} \mu_B$ and $\mu = 10^{-9} \mu_B$, as those lie outside the temperature range shown in the plot (at higher and lower temperatures, respectively). For the largest values of μ in the plot, ΔN_{eff} quickly reaches a saturation limit corresponding to a thermal abundance at the photon temperature. The drop in $\Delta N_{\text{eff}}(T)$ at later times is due to entropy injection in the plasma happening after the decoupling of RH neutrinos (particularly evident is the drop at the QCD phase transition, $T_{\text{QCD}} \approx 150$ MeV). In this regime, the final abundance is thus basically set by the decoupling temperature.

For lower values of μ ($\mu \lesssim 10^{-11} \mu_B$ for $T_{\text{in}} = 100$ GeV), RH neutrinos do not have enough time to thermalize. In this regime ΔN_{eff} decreases with decreasing μ due both to entropy production and a smaller RH population. As expected, ΔN_{eff} becomes negligibly small for vanishing μ . In the plot we also include the case for $\mu = 10^{-11} \mu_B$ and $T_{\text{in}} = 1$ GeV, shown as a dashed red line. The lower initial temperature implies that, despite the rapid initial growth, ΔN_{eff} remains significantly smaller than the contribution obtained for the same value of μ , but with $T_{\text{in}} = 100$ GeV (solid red line).

In the following, we take the “late-time” value of $\Delta N_{\text{eff}}(T)$ as the one relevant for cosmological observations. $\Delta N_{\text{eff}}(T)$ is constant for $T \lesssim 10$ MeV since no significant production of RH neutrinos takes place after that time, and the comoving density of active neutrinos does not change in the limit of instantaneous decoupling.³ We then use $\Delta N_{\text{eff}}(T = 10 \text{ MeV})$ as the late-time value of ΔN_{eff} .

³Neutrino decoupling is not instantaneous, implying that neutrinos actually benefit from a small fraction of entropy release from electron-positron annihilation. Neglecting this effect does not change significantly our results.

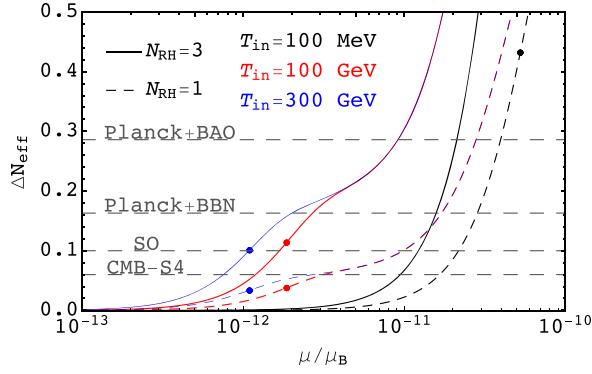


FIG. 3. The late-time value of ΔN_{eff} due to the population of three (solid) or one (dashed) species of RH neutrinos as a function of μ for different initial temperatures, enlarged in the region where $\Delta N_{\text{eff}} < 0.5$. The horizontal dashed lines indicate the current 95% bound (Planck + baryon acoustic oscillations (BAO) and Planck + BBN) and the 2σ sensitivity of future experiments (Simons Observatory (SO) and CMB-S4). The dots mark the values of μ giving $\langle \Gamma \rangle / H = 1$ at $T = T_{\text{in}}$.

IV. CONSTRAINTS ON THE NMM

In Fig. 3 we report the late-time value of ΔN_{eff} as a function of μ for different initial temperatures ($T_{\text{in}} = 100$ MeV in black, $T_{\text{in}} = 100$ GeV in red, $T_{\text{in}} = 300$ GeV in blue), in the case of one (dashed lines) or three (solid lines) species of RH neutrinos. We can identify three main regions, depending on the size of μ . As expected, in the limit of very large μ , the RH population remains coupled to the active neutrino species until late times, hence providing a large contribution to N_{eff} . For lower values of μ , RH neutrinos are still in thermal equilibrium with the plasma at early times, but the decoupling happens earlier. In this scenario, RH neutrinos are efficiently diluted by entropy production, and their contribution to N_{eff} is smaller. For even smaller values of μ , RH neutrinos are never in thermal equilibrium with the active species. A residual nonthermal population can then develop and contribute very feebly, yet nonvanishingly, to N_{eff} . As further discussed in Appendix B, the results that we obtain for N_{eff} in both the limits of large and small μ are different from the ones obtained in Ref. [25], since we do not employ the instantaneous decoupling approximation, nor do we assume *a priori* that RH neutrinos are in thermal equilibrium with the primeval plasma. Precisely, since Γ/H scales linearly with T , sizable entropy transfer from the Standard Model (SM) plasma to the RH neutrinos can take place for quite some time after the decoupling, implying that the approximation of instantaneous decoupling is particularly crude. Thus, neglecting entropy production happening after decoupling can severely underestimate the value of ΔN_{eff} associated to a given value of the NMM. Concerning the assumption of thermal equilibrium, one might argue that since Γ/H increases at high temperatures, the condition for equilibrium $\Gamma/H \gg 1$ can always be met at some very early

time. This argument, however, requires to be addressed more carefully. There are several reasons why an extrapolation to very high energies might be inappropriate. First, from a strictly observational point of view, we have no information about the cosmic thermal history above the BBN energy scale. Second, new physics might play a role above the electroweak scale, altering the thermal evolution of the plasma. Finally, our effective description of the neutrino-photon coupling induced by the NMM is expected to break down at some high energy scale, that depends on the physics inducing the NMM. Thus, it is not granted that one can always take T_{in} large enough for thermal equilibrium to be established. Solving the Boltzmann equation with vanishing initial RH population, we are able to describe the scenario in which thermal equilibrium is established, as well as the scenario in which the interactions are not strong enough to generate a thermal population. In Fig. 3 we mark with small circles the values of μ that yield $\langle \Gamma \rangle / H = 1$ at the initial temperature. To the right of the circles, $\langle \Gamma \rangle / H > 1$ at T_{in} , corresponding to the thermal regime. All curves overlap in the right part, where the final abundance of RH neutrinos is independent of T_{in} since $T_d \ll T_{\text{in}}$. Conversely, the region to the left of the circles traces the freeze-in regime, $\langle \Gamma \rangle / H < 1$ at T_{in} .

With our approach we are able to smoothly compute the value of ΔN_{eff} as a function of the NMM and compare it with observations to set constraints. The horizontal dashed lines in Fig. 3 represent the 95% Bayesian credible upper bounds on ΔN_{eff} from a combination of current cosmological data (observations of CMB anisotropies from Planck, combined with BAO, from a compilation of large-scale-structure surveys [32], and BBN data [33])⁴ and the expected 2σ sensitivity on ΔN_{eff} from future CMB surveys (SO [34] and CMB-S4 [35]). Assuming $T_{\text{in}} = 100$ MeV (black line in Fig. 3) current measurements probe the thermal regime and imply

$$\begin{aligned} \mu &< 2.1 \times 10^{-11} \mu_B && (\text{Planck} + \text{BAO}), \\ \mu &< 1.6 \times 10^{-11} \mu_B && (\text{Planck} + \text{BBN}). \end{aligned} \quad (11)$$

However, the value of T_{in} is somewhat arbitrary and can affect the final abundance. Values of $T_{\text{in}} > 100$ MeV can be safely assumed, provided that other particle species heavier than electrons and positrons are included in the plasma. Therefore, it is necessary to follow the RH neutrino thermalization across a large temperature range, from T_{in} to today, by properly taking into account the charged particle species contributing to the RH neutrino production. At this regard, the formalism discussed in Sec. II and the use of the Boltzmann equation allow us to accurately reconstruct the evolution of ΔN_{eff} due to the population of RH neutrinos

⁴The current 95% credible interval for N_{eff} from Planck + BAO is $N_{\text{eff}} = 2.99^{+0.34}_{-0.33}$ [32] and for Planck + BBN is $N_{\text{eff}} = 2.83 \pm 0.38$ [33].

produced starting from $T_{\text{in}} > 10$ MeV. This represents the main improvement of this work compared to previous literature [24]. Taking $T_{\text{in}} = 100$ GeV (red line) as our benchmark, current bounds become

$$\begin{aligned}\mu &< 9.1 \times 10^{-12} \mu_B && (\text{Planck} + \text{BAO}), \\ \mu &< 2.6 \times 10^{-12} \mu_B && (\text{Planck} + \text{BBN}).\end{aligned}\quad (12)$$

Future cosmological data will instead go deep into the freeze-in regime, for three RH neutrino families, and test values as low as $\mu = 1.7 \times 10^{-12} \mu_B$ (SO) and $\mu = 1.2 \times 10^{-12} \mu_B$ (CMB-S4). The formalism developed here allows us to constrain even such low values of the neutrino magnetic moment, which do not lead to the establishment of a thermal population of RH neutrinos. A detailed comparison with the results obtained in the previous literature can be found in Appendix B.

V. DISCUSSION AND CONCLUSIONS

In this work, we have revisited the calculation of the RH neutrino production in the early Universe, extensively discussing the cosmological implications and computing current bounds and sensitivities of future cosmological surveys on the neutrino magnetic moment μ . As mentioned in Sec. IV, one key aspect of the cosmological analysis presented here is that the choice of T_{in} is somehow arbitrary: it can be as large as the highest reheating temperature T_{RH} currently allowed by the nonobservation of primordial B -modes in the CMB. Assuming a perfectly efficient reheating and instantaneous thermalization of standard model particles after inflation, $T_{\text{in}} \sim T_{\text{RH}} \sim V^{1/4} < 1.6 \times 10^{16}$ GeV [36], V being the energy density at inflation.

In the thermal regime, the final RH abundance only depends on the value of $g_{*,s}$ at decoupling, and increasing T_{in} above 100 GeV does not change the Planck + BAO bound on μ , while it slightly affects the Planck + BBN bound, assuming no other species beyond the particle content of the standard model; compare the red and blue lines in Fig. 3. The freeze-in abundance is instead proportional to $\mu^2 T_{\text{in}}$ for constant $g_{*,s}$, as shown in Appendix A. The future sensitivity on μ will then increase for $T_{\text{in}} > 100$ GeV, scaling as $1/\sqrt{T_{\text{in}}}$ ⁵. Note, however, that the effective interaction Lagrangian in Eq. (1) will break down above some energy threshold determined by the physics governing the magnetic moment, and other assumptions made in our calculation could fail for $T_{\text{in}} \gg 100$ GeV. For example, several theories beyond the standard model predict new degrees of freedom that

⁵We have explicitly checked that when deriving constraints on μ using the rates computed at 10^3 GeV, we find $\mu < 4.3 \times 10^{-13} \mu_B$ for CMB-S4, in line with the expected $\sqrt{10}$ improvement.

could contribute to $g_{*,s}$ at those temperatures. Furthermore, the spin-flip rate in Eq. (2) assumes thermal equilibrium of the standard model plasma. Though possible (see, e.g., Refs. [37–39]), a quick, effectively instantaneous, thermalization of the standard model plasma after reheating is not guaranteed, as it depends on the details of the inflation model. A careful extension of the formalism laid down in this work is therefore required to project the sensitivity on μ in the regime $T_{\text{in}} \gg 100$ GeV.

Moreover, it cannot be excluded that the Universe underwent other reheating episodes beyond the one associated to the end of inflation. In fact, the latest of such reheating events can happen at a temperature T_{RH} as low as a few MeV without contradicting available observations [40]. The final abundance is reduced for $T_{\text{in}} \sim T_{\text{RH}} \leq T_d$, resulting in looser constraints on μ ; see, e.g., the $T_{\text{in}} = 100$ MeV curve in Fig. 3. Our choice of $T_{\text{in}} = 100$ GeV amounts to assume a standard thermal history at $T \leq 100$ GeV and that the physics responsible for the generation of neutrino magnetic moment lies at or above the electroweak scale.

In order to better understand the role of the initial temperature, in Fig. 4 we plot current constraints and discovery potentials for μ assuming that production of RH neutrinos begins at an arbitrary energy scale $\Lambda \equiv T_{\text{in}}$. There are two main ways to interpret this plot. If one assumes that the physics generating the magnetic moment lies well

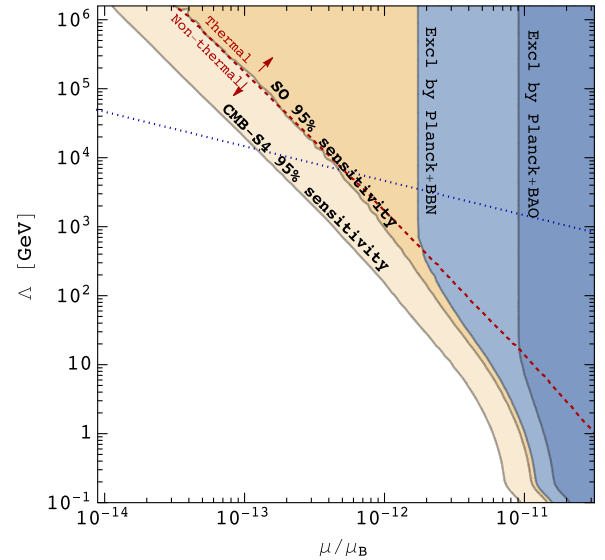


FIG. 4. Current constraints (blue) and discovery potential of future experiments (orange) in the (Λ, μ) plane, where Λ is the energy scale at which production of RH neutrinos begins. The red dashed line separates the regions of thermal and nonthermal production. The yield of RH neutrinos is practically independent of Λ above this line. The blue dotted line shows the prediction $\mu \sim m_X / (16\pi^2 \Lambda^2)$ for the magnetic moment generated by new physics at the scale Λ , mediated by a charged heavy fermion with mass $m_X = 1$ GeV [41].

above the energy scale associated to reheating, then Λ can be identified with T_{RH} . Otherwise, Λ can be identified with the scale of the new physics itself. Note that in this case the constraints shown in Fig. 4 are conservative, since we are neglecting any production that might have occurred at $T > \Lambda$. The red dashed line in the figure separates the regions of thermal and nonthermal production⁶ and clearly shows how next generation experiments will probe the nonthermal regime. In Fig. 4 the blue regions are probed by current data (Planck + BAO, Planck + BBN). It is possible to note that these exclusion regions are independent of Λ when crossing the dashed red line, denoting the condition of equilibrium. Reasonably, from the particle physics point of view, we expect $\Lambda \gtrsim 10^3$ GeV, while cosmological observations allow for a nonstandard thermal history for $\Lambda \gtrsim 10$ MeV. In this context, future cosmological probes such as SO and CMB-S4, whose sensitivities are represented by the orange regions, will be capable of fully exploring the nonthermal production of RH neutrinos, shedding light on the possible new physics above Λ .

We remark that the constraints discussed here are irreducible, since they are obtained neglecting additional nonstandard interactions between neutrinos and other, perhaps exotic, particles. Indeed, these interactions, required to justify a neutrino magnetic moment larger than the standard model prediction, $\mu \gg \mathcal{O}(10^{-19} \mu_B)$, might contribute to the RH neutrino production in the early Universe, increasing the value of ΔN_{eff} .

ACKNOWLEDGMENTS

We thank Edoardo Vitagliano and Damiano Fiorillo for helpful comments on the draft and Patrick Stengel for useful feedback on the thermalization after reheating. We warmly thank Shao-Ping Li and Xun-Jie Xu for discussion and comparison with their recent work [25]. This article/publication is based upon work from COST Action COSMIC WISPerS CA21106, supported by COST (European Cooperation in Science and Technology). We are grateful to Alessandro Mirizzi for his contributions in the initial stages of the project. The work of P.C. is supported by the European Research Council under Grant No. 742104 and by the Swedish Research Council (VR) under Grants No. 2018-03641 and No. 2019-02337. G.L. is supported by the European Union's Horizon 2020 Europe research and innovation programme under the Marie Skłodowska-Curie Grant Agreement No. 860881-HIDDeN. M.G. and M.L. acknowledge support from the COSMOS network [42] through the ASI (Italian Space Agency) Grants No. 2016-24-H.0, No. 2016-24-H.1-2018, and No. 2019-9-HH.0. We acknowledge the use of

⁶In more detail, the red dashed line corresponds, for each μ , to the initial temperature that gives a yield equal, within 1%, to the yield that would be obtained in the limit $T_{\text{in}} \rightarrow \infty$ (i.e., for $T_{\text{in}} \gg T_d$).

CINECA HPC resources from the InDark project in the framework of the INFN-CINECA agreement.

APPENDIX A: DETAILS ON THE FREEZE-IN REGIME

In the freeze-in regime, it is possible to derive the explicit dependence of ΔN_{eff} on μ and the initial temperature T_{in} and far from entropy production events, when the equilibrium distribution does not depend on time, i.e., $f^{\text{eq}}(q, t) = f^{\text{eq}}(q)$. Introducing the deviation from equilibrium $\Delta f(q, t) \equiv f^R(q, t) - f^{\text{eq}}(q)$, it is straightforward to write a formal solution of the Boltzmann equation,

$$\begin{aligned} \Delta f(q, t) &= -f^{\text{eq}}(q) \exp \left[- \int_{t_{\text{in}}}^t \Gamma dt' \right] \\ &= -f^{\text{eq}}(q) \exp \left[- \int_z^{z_{\text{in}}} \frac{\Gamma}{H(1+z')} dz' \right], \end{aligned} \quad (\text{A1})$$

where we use $q = ap$ as the momentum variable to ensure that $\partial_t f^{\text{eq}} = 0$, and the initial condition $\Delta f(q, t_{\text{in}}) = -f^{\text{eq}}(q)$ because we assume a vanishing initial population of RH neutrinos. In the following, we will use the subscript “in” to denote quantities evaluated at the initial time. We now write the RH neutrino production rate as

$$\Gamma = \alpha \mu^2 \sqrt{g_{*,s}(T)} T^3 \tilde{\Gamma}(y, T), \quad (\text{A2})$$

where the momentum variable is $y = p/T = q/aT$. Note that $\tilde{\Gamma}$ does not depend on the temperature far from entropy production events, and its temperature dependence is, anyway, very mild, even when accounting for entropy production (see the lower panel in Fig. 1).

Using the expression for the Hubble rate in the radiation-dominated era, we can recast the integral in Eq. (A1) as

$$\begin{aligned} \int_z^{z_{\text{in}}} \frac{\Gamma}{H(1+z')} dz' &= \sqrt{\frac{45}{4\pi^3}} \alpha \mu^2 m_{\text{pl}} \int_z^{z_{\text{in}}} \frac{\tilde{\Gamma} T}{1+z} dz' \simeq \\ &\simeq \sqrt{\frac{45}{4\pi^3}} \alpha \mu^2 m_{\text{pl}} (\tilde{\Gamma} T) \Big|_{z_{\text{in}}} = \frac{\Gamma}{H} \Big|_{z_{\text{in}}}, \end{aligned} \quad (\text{A3})$$

where the approximate equality holds for $z \ll z_{\text{in}}$ and when the initial time is far from entropy production events. Precisely, since $T/(1+z) \propto g_{*,s}(T)$ and $\tilde{\Gamma}$ itself is weakly dependent on temperature, the integrand varies significantly only in proximity of entropy production events, and the value of the integral is dominated by the high-temperature contribution. Note the somehow fortunate cancellation between the factors of $\sqrt{g_{*,s}}$ in Γ and H , since the effective number of degrees of freedom for energy density $g_{*,r} = g_{*,s}$ for $T \gg 1$ MeV.

Since we are focusing on the freeze-in regime, $\Gamma/H \ll 1$. From the above discussion, the requirement that this

inequality holds at T_{in} guarantees that it also holds at $z < z_{\text{in}}$, and that its integrated value over $d\ln(1+z)$ is itself much smaller than 1. In terms of μ and T_{in} , the condition $\Gamma_{\text{in}}/H_{\text{in}} \ll 1$ reads

$$0.47 \times \left(\frac{\mu}{10^{-12} \mu_B} \right)^2 \left(\frac{T_{\text{in}}}{100 \text{ GeV}} \right) \tilde{\Gamma}_{\text{in}} \ll 1. \quad (\text{A4})$$

We can thus expand the exponential in Eq. (A1) to first order in its argument and then compute ΔN_{eff} . This yields, for a single species of RH neutrinos,

$$\Delta N_{\text{eff}}(T \ll T_{\text{in}}) = \frac{120}{7\pi^4} \left(\frac{g_{*,s}(T)}{g_{*,s}(T_{\text{in}})} \right)^{4/3} \int_0^\infty dy y^3 \frac{\Gamma_{\text{in}}}{H_{\text{in}}} f^{\text{eq}}, \quad (\text{A5})$$

where $\Gamma_{\text{in}} = \Gamma(y, T_{\text{in}})$. The temperature dependence of the right-hand side is encoded in the $g_{*,s}^{4/3}$ factor and can be understood as follows. In the freeze-in regime, the production of RH neutrinos mostly happens at high temperatures, thus the RH abundance quickly saturates shortly after the initial time and stays constant for $T \ll T_{\text{in}}$. The energy density of RH neutrinos relative to the active ones can only change when more active neutrinos are produced due to entropy injection in the plasma. Substituting the explicit expression of $\Gamma_{\text{in}}/H_{\text{in}}$ with the one shown in Eq. (A3), we obtain

$$\Delta N_{\text{eff}} = \frac{120}{7\pi^4} \sqrt{\frac{45}{4\pi^3}} \alpha \mu^2 T_{\text{in}} m_{\text{pl}} \times \left(\frac{g_{*,s}(T)}{g_{*,s}(T_{\text{in}})} \right)^{4/3} \int_0^\infty dy y^3 \tilde{\Gamma}_{\text{in}} f^{\text{eq}}. \quad (\text{A6})$$

This quantity depends on the initial temperature through the explicit factor $T_{\text{in}} g_{*,s}(T_{\text{in}})^{-4/3}$ and also through the integrand. However, when $g_{*,s}$ is constant, this dependence reduces to the only factor T_{in} . In this regime, $\Delta N_{\text{eff}} \propto \mu^2 T_{\text{in}}$. Thus, a given observational bound on ΔN_{eff} translates, in the freeze-in regime defined by Eq. (A4), to a bound on $\mu^2 T_{\text{in}}$. In other words, constraints on μ in the freeze-in regime scale as $T_{\text{in}}^{-1/2}$. Note that, since $\Gamma/H \propto \mu^2 T$, the decoupling temperature scales as μ^{-2} . This ensures that, for constant $g_{*,s}$, the rescaled constraint will still correspond to the freeze-in regime. To illustrate this, let us consider an initial temperature in the freeze-in regime, $T_{\text{in}} \ll T_d$, and the associated constraint $\mu < \bar{\mu}$. Rescaling T_{in} to $T'_{\text{in}} > T_{\text{in}}$ would produce a new upper bound (assuming freeze-in) $\bar{\mu}' = \bar{\mu} \sqrt{\frac{T_{\text{in}}}{T'_{\text{in}}}}$. Since the decoupling temperature T'_d associated to $\bar{\mu}'$ is $T'_d = T_d \frac{\bar{\mu}^2}{\bar{\mu}'^2}$, we find that $T'_{\text{in}}/T'_d = T_{\text{in}}/T_d \ll 1$.

APPENDIX B: IMPACT OF THE DIFFERENT COSMOLOGICAL ANALYSES

Here we discuss modeling assumptions and approximations that enter the computation of N_{eff} and subsequent bounds on the NMM. We find it useful, for the purpose of this discussion, to show in Fig. 5 the value of N_{eff} for three RH neutrinos as a function of μ , as obtained with different approaches. The black, red, and blue curves have been obtained by direct integration of the Boltzmann equation, for three different initial temperatures, namely $T_{\text{in}} = 100 \text{ GeV}$, $T_{\text{in}} = 10^6 \text{ GeV}$, and $T_{\text{in}} = 100 \text{ MeV}$, respectively, and assuming a vanishing population of RH neutrinos at the initial time.

First, we compare our results with those of Ref. [24], where the primeval plasma is composed only by electrons and positrons, restricting the analysis to temperatures $T \leq m_\mu \simeq 100 \text{ MeV}$. A bound $\mu \lesssim 6.2 \times 10^{-11} \mu_B$ was derived by requiring that RH neutrinos have already decoupled from the thermal bath at the highest temperature considered in the analysis, i.e., $\Gamma < H$ at $T = 100 \text{ MeV}$, with Γ the thermally-averaged interaction rate. Since a species decoupling after $\mu^+ \mu^-$ annihilation is at a temperature equal or larger than the active neutrinos, this amounts to requiring that each RH neutrino species contributes with $\Delta N_{\text{eff}} < 1$ to the radiation density. Applying the same criterion ($\Gamma < H$ at 100 MeV) using our own calculation of the rate, we obtain $\mu < 5.3 \times 10^{-11} \mu_B$, as represented by the blue dot in Fig. 5, roughly in good agreement with Ref. [24].

Current observations constrain $\Delta N_{\text{eff}} < 0.286$ (Planck + BAO), leading to a stronger bound on μ . Indeed, ignoring any production that might have happened at epochs earlier than $T \simeq 100 \text{ MeV}$, as implicitly done in Ref. [24], would yield $\mu \lesssim 2.1 \times 10^{-11} \mu_B$, as shown by the blue curve in Fig. 5. However, the value of T_{in} is somehow

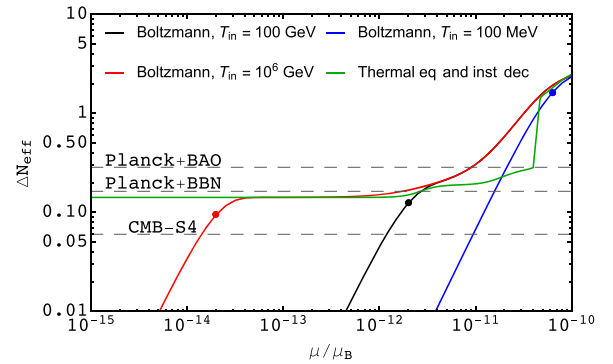


FIG. 5. Late-time value of ΔN_{eff} due to the population of three species of RH neutrinos as function of μ for different initial temperatures and calculation methods (see text for details). The horizontal dashed lines indicate the current 95% bound (Planck + BAO and Planck + BBN) and the 2σ sensitivity of future experiments (CMB-S4). The dots mark the values of μ giving thermal equilibrium at the initial temperature $T = T_{\text{in}}$.

arbitrary and can affect the final abundance. Values of $T_{\text{in}} > 100$ MeV can be considered, provided that other particle species in the plasma are included. This is the main improvement of this work. For $T_{\text{in}} = 100$ GeV (the black curve in Fig. 5) we obtain the bound

$$\mu \lesssim 9.1 \times 10^{-12} \mu_B. \quad (\text{B1})$$

Notice that this result corresponds to full thermalization at $T \gtrsim 4$ GeV. Therefore, this is insensitive to further increases of the initial temperature above 100 GeV, as confirmed by the $T_{\text{in}} = 10^6$ GeV case (i.e., by noting that the black and red curves in Fig. 5 overlap in the region constrained by the Planck + BAO dataset).

The dataset combination Planck + BBN prefers smaller values of N_{eff} than Planck + BAO, albeit with a slightly large uncertainty and, as a result, provides the stronger constraint $\Delta N_{\text{eff}} \lesssim 0.163$, leading to $\mu < 2.7 \times 10^{-12} \mu_B$ for $T_{\text{in}} = 100$ GeV. In this case, the largest allowed value of μ corresponds to thermal equilibrium at $T \gtrsim 50$ GeV, which is fairly close to T_{in} . We can thus expect that the bound will saturate for a somehow larger choice of the initial temperature. This can be concluded by noting that the black and red curves in Fig. 5 start to diverge for values of the NMM close to the upper bound. Indeed, we have explicitly verified that the bound saturates at $\mu < 1.7 \times 10^{-12} \mu_B$ for large enough values of T_{in} , as shown by the red line.

We now comment on the difference between the green line and the other cases previously discussed. In our analysis, we follow the decoupling of the RH neutrinos by solving the relevant Boltzmann equation with vanishing initial population and for different values of the initial temperature T_{in} . This yields the black, red, and blue lines in Fig. 5 for $T_{\text{in}} = 100$ GeV, $T_{\text{in}} = 10^6$ GeV, and $T_{\text{in}} = 100$ MeV, respectively, as detailed before. A different approach, used, e.g., in Ref. [25], would consist in assuming that a thermal population is established at early times and that decoupling happens instantaneously at the time when $\Gamma/H = 1$. One should then use entropy conservation to find the ratio between the RH and photon temperatures at late times and compute the corresponding value of ΔN_{eff} . This yields the green line in Fig. 5.

The first difference between the two approaches is related to the instantaneous decoupling approximation, as evident by comparing the black and green lines in Fig. 5. Before commenting further on the origin of this difference, we discuss the effects on the NMM bounds. The initial temperature for the red curve, $T_{\text{in}} = 10^6$ GeV, has been chosen to correspond to thermal equilibrium for $\mu \gtrsim 2 \times 10^{-14} \mu_B$, as represented by the red dot, so that the differences between the two curves at larger values of the NMM are due to the treatment of decoupling. It can be clearly seen in Fig. 5 that the instantaneous decoupling can

significantly underestimate the value of ΔN_{eff} , and thus lead to (artificially) looser constraints on μ . For Planck + BAO, the constraint would go from $\mu < 9.1 \times 10^{-12} \mu_B$ to $\mu < 3.7 \times 10^{-11} \mu_B$. For Planck + BBN, the constraint would go from $\mu < 1.7 \times 10^{-12} \mu_B$ to $\mu < 2.6 \times 10^{-12} \mu_B$. The latter value matches very closely the bound quoted in Ref. [25], $\mu < 2.7 \times 10^{-12} \mu_B$, as expected given that it has been obtained under the same assumptions. This bound is also very close to the one we found using the full Boltzmann approach for $T_{\text{in}} = 100$ GeV (black line). This agreement should be, however, regarded as accidental, as it is clear that the black and green curves in Fig. 5 have different behaviors, and only by chance cross at a value of ΔN_{eff} corresponding to the Planck + BBN bound.

Given that Γ/H scales linearly with T , sizable entropy transfer from the SM plasma to the RH neutrinos can take place for quite some time after the condition $\Gamma/H = 1$ is realized at the decoupling temperature T_{dec} , i.e., the approximation of instantaneous decoupling is particularly crude. Thus, neglecting entropy production happening after decoupling, at $T < T_{\text{dec}}$, can severely underestimate the value of ΔN_{eff} associated to a given value of the NMM. This explains the discrepancy between the black and green lines. The solution obtained by solving the Boltzmann equation with the full temperature dependence of Γ/H (red curve) clearly differs in the region of $10^{-12} \mu_B \lesssim \mu \lesssim 5 \times 10^{-11} \mu_B$. This is particularly important since this is exactly the region probed by currently available data. Note also that solving the Boltzmann equation leads to a much smoother behavior for $\Delta N_{\text{eff}}(\mu)$, making the results obtained in this approach less dependent on the modeling of the expansion and interaction rates around the time of QCD decoupling.

One might naively expect that, since Γ/H increases at large temperatures, the equilibrium condition $\Gamma/H \gg 1$ can be always met in the early Universe. However, several factors might affect this extrapolation to high temperatures. From an observational standpoint, there are direct probes of the cosmological history only below the BBN energy scale. Additionally, new physics might appear above the electroweak scale, potentially altering the primeval plasma. Moreover, the NMM interaction is an effective description valid up to a certain high energy threshold, depending on the physics inducing the NMM. Hence, it cannot be assumed that the parameter T_{in} can always be set sufficiently high to establish thermal equilibrium. By resolving the Boltzmann equation with a vanishing initial RH neutrino population, we are able to both describe the scenario in which thermal equilibrium is established, as well as the scenario in which the interactions are not strong enough to generate a thermal population.

- [1] C. L. Cowan and F. Reines, Neutrino magnetic moment upper limit, *Phys. Rev.* **107**, 528 (1957).
- [2] F. Reines, H. S. Gurr, and H. W. Sobel, Detection of $\bar{\nu}_e - e$ scattering, *Phys. Rev. Lett.* **37**, 315 (1976).
- [3] H. B. Li *et al.* (TEXONO Collaboration), Limit on the electron neutrino magnetic moment from the Kuo-Sheng reactor neutrino experiment, *Phys. Rev. Lett.* **90**, 131802 (2003).
- [4] Z. Daraktchieva *et al.* (MUNU Collaboration), Limits on the neutrino magnetic moment from the MUNU experiment, *Phys. Lett. B* **564**, 190 (2003).
- [5] A. I. Derbin, A. V. Chernyi, L. A. Popeko, V. N. Muratova, G. A. Shishkina, and S. I. Bakhlanov, Experiment on anti-neutrino scattering by electrons at a reactor of the Rovno nuclear power plant, *JETP Lett.* **57**, 768 (1993).
- [6] M. Deniz *et al.* (TEXONO Collaboration), Constraints on non-standard neutrino interactions and unparticle physics with neutrino-electron scattering at the Kuo-Sheng nuclear power reactor, *Phys. Rev. D* **82**, 033004 (2010).
- [7] A. G. Beda, V. B. Brudanin, V. G. Egorov, D. V. Medvedev, V. S. Pogosov, M. V. Shirchenko, and A. S. Starostin, The results of search for the neutrino magnetic moment in GEMMA experiment, *Adv. High Energy Phys.* **2012**, 350150 (2012).
- [8] M. Agostini *et al.* (Borexino Collaboration), Limiting neutrino magnetic moments with Borexino Phase-II solar neutrino data, *Phys. Rev. D* **96**, 091103 (2017).
- [9] E. Aprile *et al.* (XENON Collaboration), Search for new physics in electronic recoil data from XENONnT, *Phys. Rev. Lett.* **129**, 161805 (2022).
- [10] K. Fujikawa and R. Shrock, The magnetic moment of a massive neutrino and neutrino spin rotation, *Phys. Rev. Lett.* **45**, 963 (1980).
- [11] R. Barbieri and G. Fiorentini, The solar neutrino puzzle and the neutrino (L) \rightarrow neutrino (R) conversion hypothesis, *Nucl. Phys.* **B304**, 909 (1988).
- [12] N. F. Bell, V. Cirigliano, M. J. Ramsey-Musolf, P. Vogel, and M. B. Wise, How magnetic is the Dirac neutrino?, *Phys. Rev. Lett.* **95**, 151802 (2005).
- [13] S. Davidson, M. Gorbahn, and A. Santamaria, From transition magnetic moments to Majorana neutrino masses, *Phys. Lett. B* **626**, 151 (2005).
- [14] N. F. Bell, M. Gorchtein, M. J. Ramsey-Musolf, P. Vogel, and P. Wang, Model independent bounds on magnetic moments of Majorana neutrinos, *Phys. Lett. B* **642**, 377 (2006).
- [15] A. Heger, A. Friedland, M. Giannotti, and V. Cirigliano, The impact of neutrino magnetic moments on the evolution of massive stars, *Astrophys. J.* **696**, 608 (2009).
- [16] F. Capozzi and G. Raffelt, Axion and neutrino bounds improved with new calibrations of the tip of the red-giant branch using geometric distance determinations, *Phys. Rev. D* **102**, 083007 (2020).
- [17] R. Barbieri and R. N. Mohapatra, Limit on the magnetic moment of the neutrino from supernova SN 1987a observations, *Phys. Rev. Lett.* **61**, 27 (1988).
- [18] R. Barbieri, R. N. Mohapatra, and T. Yanagida, The magnetic moment of the neutrino and its implications for neutrino signal from SN1987A, *Phys. Lett. B* **213**, 69 (1988).
- [19] D. Notzold, New bounds on neutrino magnetic moments from stellar collapse, *Phys. Rev. D* **38**, 1658 (1988).
- [20] J. A. Morgan, Anomalous neutrino interactions and primordial nucleosynthesis, *Mon. Not. R. Astron. Soc.* **195**, 173 (1981).
- [21] J. A. Morgan, Cosmological upper limit to neutrino magnetic moments, *Phys. Lett.* **102B**, 247 (1981).
- [22] M. Fukugita and S. Yazaki, Reexamination of astrophysical and cosmological constraints on the magnetic moment of neutrinos, *Phys. Rev. D* **36**, 3817 (1987).
- [23] A. Loeb and L. Stodolsky, Relativistic spin relaxation in stochastic electromagnetic fields, *Phys. Rev. D* **40**, 3520 (1989).
- [24] P. Elmfors, K. Enqvist, G. Raffelt, and G. Sigl, Neutrinos with magnetic moment: Depolarization rate in plasma, *Nucl. Phys.* **B503**, 3 (1997).
- [25] S.-P. Li and X.-J. Xu, Neutrino magnetic moments meet precision N_{eff} measurements, *J. High Energy Phys.* **02** (2023) 085.
- [26] H. A. Weldon, Covariant calculations at finite temperature: The relativistic plasma, *Phys. Rev. D* **26**, 1394 (1982).
- [27] G. Mangano, G. Miele, S. Pastor, and M. Peloso, A precision calculation of the effective number of cosmological neutrinos, *Phys. Lett. B* **534**, 8 (2002).
- [28] P. F. de Salas and S. Pastor, Relic neutrino decoupling with flavour oscillations revisited, *J. Cosmol. Astropart. Phys.* **07** (2016) 051.
- [29] K. Akita and M. Yamaguchi, A precision calculation of relic neutrino decoupling, *J. Cosmol. Astropart. Phys.* **08** (2020) 012.
- [30] J. J. Bennett, G. Buldgen, P. F. De Salas, M. Drewes, S. Gariazzo, S. Pastor, and Y. Y. Y. Wong, Towards a precision calculation of N_{eff} in the Standard Model II: Neutrino decoupling in the presence of flavour oscillations and finite-temperature QED, *J. Cosmol. Astropart. Phys.* **04** (2021) 073.
- [31] J. Froustey and C. Pitrou, Primordial neutrino asymmetry evolution with full mean-field effects and collisions, *J. Cosmol. Astropart. Phys.* **03** (2022) 065.
- [32] N. Aghanim *et al.* (Planck Collaboration), Planck 2018 results. VI. Cosmological parameters, *Astron. Astrophys.* **641**, A6 (2020); **652**, C4(E) (2021).
- [33] B. D. Fields, K. A. Olive, T.-H. Yeh, and C. Young, Big-Bang nucleosynthesis after Planck, *J. Cosmol. Astropart. Phys.* **03** (2020) 010; **11** (2020) E02.
- [34] P. Ade *et al.* (Simons Observatory Collaboration), The Simons Observatory: Science goals and forecasts, *J. Cosmol. Astropart. Phys.* **02** (2019) 056.
- [35] K. Abazajian *et al.*, CMB-S4 science case, reference design, and project plan, [arXiv:1907.04473](https://arxiv.org/abs/1907.04473).
- [36] Y. Akrami *et al.* (Planck Collaboration), Planck 2018 results. X. Constraints on inflation, *Astron. Astrophys.* **641**, A10 (2020).

- [37] S. Davidson and S. Sarkar, Thermalization after inflation, *J. High Energy Phys.* **11** (2000) 012.
- [38] K. Harigaya and K. Mukaida, Thermalization after/during reheating, *J. High Energy Phys.* **05** (2014) 006.
- [39] K. Mukaida and M. Yamada, Cascades of high-energy SM particles in the primordial thermal plasma, *J. High Energy Phys.* **10** (2022) 116.
- [40] P. F. de Salas, M. Lattanzi, G. Mangano, G. Miele, S. Pastor, and O. Pisanti, Bounds on very low reheating scenarios after Planck, *Phys. Rev. D* **92**, 123534 (2015).
- [41] X.-J. Xu, Tensor and scalar interactions of neutrinos may lead to observable neutrino magnetic moments, *Phys. Rev. D* **99**, 075003 (2019).
- [42] www.cosmosnet.it